JCTC Journal of Chemical Theory and Computation

Article

pubs.acs.org/JCTC

Modeling Excited States in TiO_2 Nanoparticles: On the Accuracy of a TD-DFT Based Description

Enrico Berardo,[†] Han-Shi Hu,[‡] Stephen A. Shevlin,[†] Scott M. Woodley,[†] Karol Kowalski,[‡] and Martijn A. Zwijnenburg*[,†]

[†]Department of Chemistry, University College London, 20 Gordon Street, WC1H 0AJ, London, United Kingdom

[‡]William R. Wiley Environmental Molecular Science Laboratory, Battelle, Pacific Northwest National Laboratory, K8-91, P.O. Box 999, Richland, Washington 99352, United States

Supporting Information

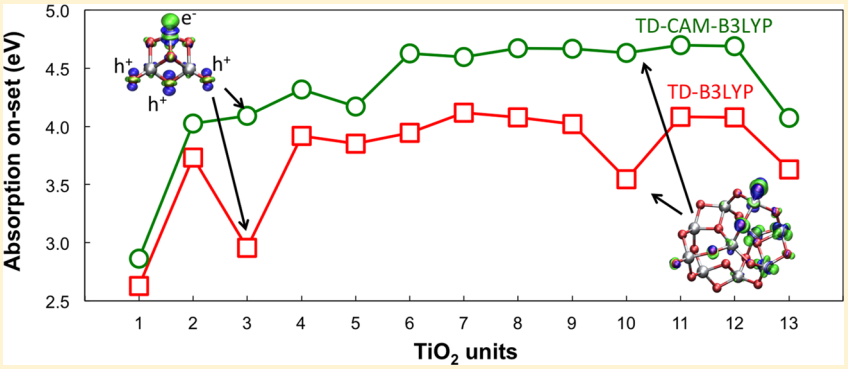

ABSTRACT: We have investigated the suitability of Time-Dependent Density Functional Theory (TD-DFT) to describe vertical low-energy excitations in naked and hydrated titanium dioxide nanoparticles. Specifically, we compared TD-DFT results obtained using different exchange-correlation (XC) potentials with those calculated using Equation-of-Motion Coupled Cluster (EOM-CC) quantum chemistry methods. We demonstrate that TD-DFT calculations with commonly used XC potentials (e.g., B3LYP) and EOM-CC methods give qualitatively similar results for most TiO_2 nanoparticles investigated. More importantly, however, we also show that, for a significant subset of structures, TD-DFT gives qualitatively different results depending upon the XC potential used and that only TD-CAM-B3LYP and TD-BHLYP calculations yield results that are consistent with those obtained using EOM-CC theory. Moreover, we demonstrate that the discrepancies for such structures originate from a particular combination of defects that give rise to charge-transfer excitations, which are poorly described by XC potentials that do not contain sufficient Hartree−Fock like exchange. Finally, we consider that such defects are readily healed in the presence of ubiquitously present water and that, as a result, the description of vertical low-energy excitations for hydrated TiO_2 nanoparticles is nonproblematic.

1. INTRODUCTION

Titanium dioxide (TiO_2) nanostructures have attracted great interest in the past few decades due to their low cost, environmental compatibility, and experimentally proven potential for photocatalytic[1−5] and photovoltaic[6] applications. In particular, the use of such nanostructures as heterogeneous catalysts for the photocatalytic splitting of water to produce renewable hydrogen[7−9] and in dye-sensitized solar cells[10] has been the subject of intense research. Recent studies[11−15] suggest that the size and the shape of TiO_2 nanostructures directly influence their performance in these applications and hence must have a clear effect on the microscopic electron−hole pair production, recombination, separation, and diffusion rates.

To understand the physics and chemistry underlying the application of TiO_2 nanostructures in photocatalysis and photovoltaics from a theoretical point of view, TiO_2 nanostructures and extended systems have been computationally extensively studied using a variety of methods.[16−31] Most of these studies employ either ground state Density Functional Theory (DFT) or its excited state variant Time-Dependent Density Functional Theory (TD-DFT). In the former case, optical excitations are generally assumed to map onto excitations from occupied to unoccupied Kohn−Sham orbitals, which is theoretically somewhat difficult to justify. Alternatively, for the lowest triplet excited state, the excitation is modeled as a state obtained self-consistently by using a ΔSCF approach. TD-DFT, in contrast, is a genuine excited state method that can be used for any number of excitations of any multiplicity. However, just like DFT in the case of the ground state, TD-DFT (and ΔSCF) suffers from the fact that the results are, to a

Received: November 26, 2013
Published: February 11, 2014

smaller or larger degree, dependent on the exchange-correlation (XC) potential used. This might be especially true for TiO_2 and other transition metal containing systems. On the other hand, correlated wave function methods used in quantum chemistry, e.g., Coupled Cluster (CC) and Complete Active Space second order Perturbation Theory (CASPT2), do not suffer from this problem and are perhaps the gold standard for excitation calculations. However, the poor scaling of such methods with the number of electrons in the system means that they can only be used for very small nanoclusters containing merely a few transition metal atoms. For example, the largest system studied to date for TiO_2 using correlated wave function methods is the $(TiO_2)_3$ trimer.[32] The majority of CC and CASPT2 simulations focused on the description of the excited states of the TiO_2 monomer.[33−35] Finally, there have also been studies on TiO_2 nanostructures using Green's function based many-body perturbation theory methods: GW and BSE.[36,37]

Here, we perform a study where we compare the performance of TD-DFT using different XC potentials with correlated wave function methods for a number of relevant nanoparticle structures, sampling a range of titanium environments such as 3-fold, 4-fold, and 5-fold coordination. We consider correlated wave function results obtained with the Equation of Motion−Coupled Cluster (EOM-CC) methods and TD-DFT results obtained with the PBE, B3LYP, CAM-B3LYP, and BHLYP XC potentials. We focus here on the performance of these methods when calculating the vertical singlet excitation spectra of the nanoparticles, the equivalent of the experimental UV−vis absorption spectra. We pay special attention to the lowest singlet excitation (S1), as this excitation, following Kasha's principle,[38] is the likely source of fluorescence (luminescence) and the state relevant to applications such as photocatalysis and photovoltaics. An accurate description of this state at the ground state geometry is, therefore, a crucial staring point for future computational work on TiO_2 nanoparticles that will focus on modeling phenomena that involve excited state relaxation, following the ideas developed by us[39−44] and others.[45−48]

In this paper, we will demonstrate that, for most of the TiO_2 nanoparticles, TD-DFT, with all the tested XC potentials and EOM-CC calculations give qualitatively similar results. Moreover, we will show that TD-DFT calculations, using the B3LYP and CAM-B3LYP XC potential, give the best quantitative fit to EOM-CC excitation energies. Importantly, however, we will also show that for an important subset of structures TD-DFT can give qualitatively different results depending on the XC potential used and that, in this case, only TD-CAM-B3LYP and TD-BHLYP calculations yield results that are qualitatively consistent with those obtained using EOM-CC theory. We will demonstrate that the discrepancies for these structures arise from a particular combination of defects, excitation involving which are poorly described by TD-PBE and TD-B3LYP. Finally, we demonstrate that these defects react exothermically with water to form hydroxyl groups and show that for hydrated TiO_2 nanoparticles the qualitative discrepancies between the different methods, observed for naked particles, disappear.

2. COMPUTATIONAL DETAILS

The geometry of each structure used in this work was optimized at the DFT level with the hybrid B3LYP[49] XC potential in conjunction with the triple-ζ def2-TZVP basis set.[50] The harmonic frequencies at the geometries of the stationary points obtained in the DFT optimizations were calculated using the same DFT setup (B3LYP/def2-TZVP level) to verify that the optimized structures correspond to proper minima on the ground state potential energy surface. The electronic ground state of all the clusters studied in this work is assumed to be a closed-shell singlet. For the naked $(TiO_2)_n$ clusters, where n = 1−8 and 10, we used the global minimum (GM, the lowest energy structure for a given cluster-size) geometries reported by a number of groups,[22,37,51−55] while for the clusters n = 9 and 11−13, we used the recent structures obtained by Chen and Dixon.[56] To investigate a larger range of titanium and oxygen coordination environments, we also examined a number of metastable isomers (i.e., local minima for a given cluster size that lie higher in energy than the GM). For the $(TiO_2)_2$ dimer, this included two metastable structures that we labeled "*cis*" and "*club*," with C_{2v} and C_s symmetry, respectively,[37,53] while for the trimer $(TiO_2)_3$ we included one higher metastable isomer with C_1 symmetry, labeled as "*alt.*"[36,37,53] The geometries of the stable and metastable structures for the n = 1−5 subset are shown in Figure 1, while the remaining n = 6−13 structures are given in section ESI-1 of the Supporting Information.

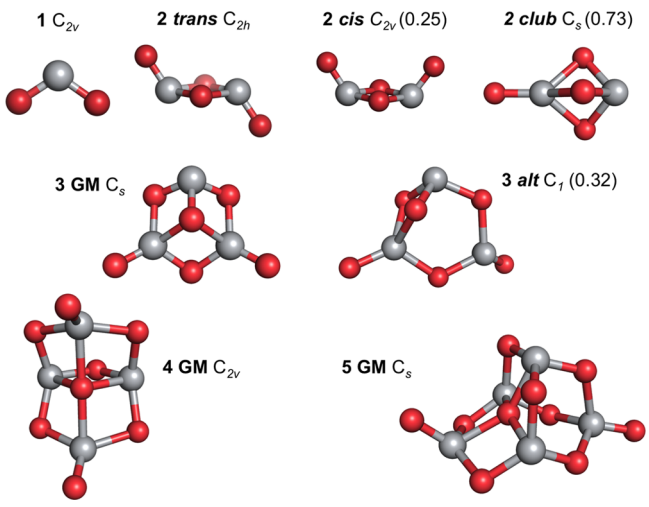

Figure 1. Global minimum (GM) atomic configurations for $(TiO_2)_n$ clusters with n = 1−5. For the dimers and trimers, metastable clusters are also shown. Labels include point group symmetry, and for the non-GM structures, the energy difference in eV relative to the GM energy calculated at the B3LYP/def2-TZVP level. Red spheres denote oxygen atoms, whereas gray spheres denote titanium atoms.

The hydrated systems, $(TiO_2)_n(H_2O)_m$ where n and m range from 1 to 3, were obtained through the saturation of all the under-coordinated titanium and oxygen atoms present in the naked clusters with hydroxyl groups and protons, respectively. Here, we assumed that titanium atoms are normally coordinated by at least four oxygen atoms and oxygen atoms form at least two bonds. The harmonic frequencies were also calculated on the DFT optimized geometries of each hydrated nanoparticle, in order to verify that they correspond to proper minima. All the hydrated clusters are shown in Figure 2. The DFT optimized structures include $Ti(OH)_4$, with S_4 symmetry; $(TiO_2)_2(H_2O)_2$, with C_{2v} symmetry; and $(TiO_2)_2(H_2O)$, $(TiO_2)_3(H_2O)_2$, and $(TiO_2)_3(H_2O)_3$, all with C_1 symmetry. The coordinates of all the structures (naked and hydrated) used in this study are listed in ESI-1 and ESI-3, respectively.

For all of the B3LYP optimized geometries, the energies of the lowest singlet excited states were obtained at the TD-DFT/

dx.doi.org/10.1021/ct4010273 | *J. Chem. Theory Comput.* 2014, 10, 1189−1199

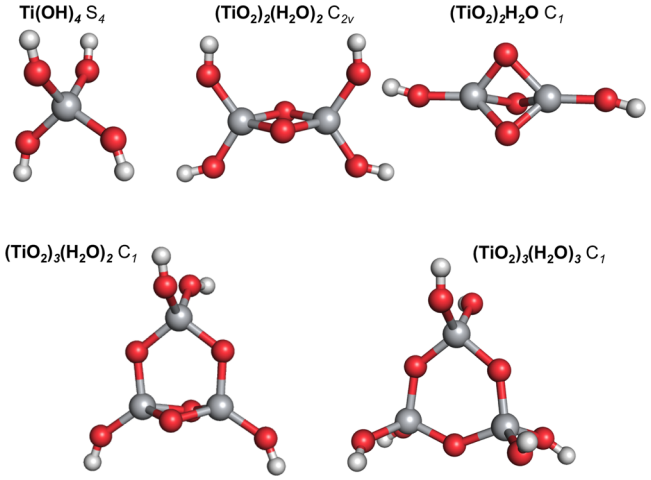

Figure 2. $(TiO_2)_n(H_2O)_m$ hydrated clusters, with n and m ranging between 1 and 3. In order to saturate relevant defects, one water molecule is added per singly coordinated oxygen atom in the originally naked clusters [with the $(TiO_2)_3(H_2O)_3$ cluster as the only exception, where one additional water molecule was added to generate the same coordination environment for all the titanium atoms]. For each cluster, the symmetry of the B3LYP/def2-TZVP minimum is given.

def2-TZVP level with different XC potentials (the pure GGA PBE,[57] the hybrids B3LYP and BHLYP,[49] and the range-separated hybrid XC potential CAM-B3LYP[58]). For selected B3LYP optimized geometries, the four lowest energy excited states were also calculated with two different coupled cluster (CC) approaches: EOM-CCSD and EOM-CCSDT,[59,60] methods already discussed in the context of TiO_2 clusters in our previous work.[32]

Due to the high computational cost required, we were not able to optimize the structures of clusters larger than the monomer with the CC approaches. However, for some clusters, we have also obtained the minimum energy geometries with the PBE and CAM-B3LYP XC potentials and calculated the respective vertical excitations. The use of B3LYP optimized structures, when compared to their fully optimized ground-state counterparts for each different XC potential, was found to introduce an average difference of 0.08 eV in the calculated excitation energies for the smaller $(TiO_2)_n$ naked clusters, where n = 1−5. Vertical excitations at these optimized geometries are listed in the Supporting Information ESI-2.

While for all TD-DFT calculations, we employed the def2-TZVP basis set, in the case of the EOM-CC methods, we used two different basis sets: the split-valence def2-SV(P) basis-set[61] and the larger triple-ζ def2-TZVPP basis set.[50] From now on, these two basis sets will be referred to as SV and TZ, respectively. All the coupled cluster calculations, for reasons of computational tractability, employed the frozen core approximation where only the valence electrons are correlated (i.e., the 1s orbitals of the oxygen atoms and the 1s to 3p orbitals of the titanium atoms are frozen).[32] Our previous work showed, in the case of the TiO_2 monomer, that the use of the frozen core approximation introduces a typical downward shift of 0.1 eV in the calculated energy relative to the all-electron CC results.

The DFT/TD-DFT calculations employing the PBE, B3LYP, and BHLYP XC potential were performed with the Turbomole 6.4 code,[62] while the TD-DFT results obtained for the CAM-B3LYP XC potential were calculated with the GAMESS US code (version 26 October 2012).[63] The coupled cluster calculations employed the Tensor Contraction Engine (TCE) module[64] of the NWChem 6.1 package.[65] The orbital overlap measure "Λ" of Peach et al.,[66] as implemented within GAMESS US, was also calculated.

For the graphic representations of the clusters studied, we used the Pymol Molecular Graphics System,[67] while VMD[68] was employed for the visualization of the differences between the ground state and excited state density.

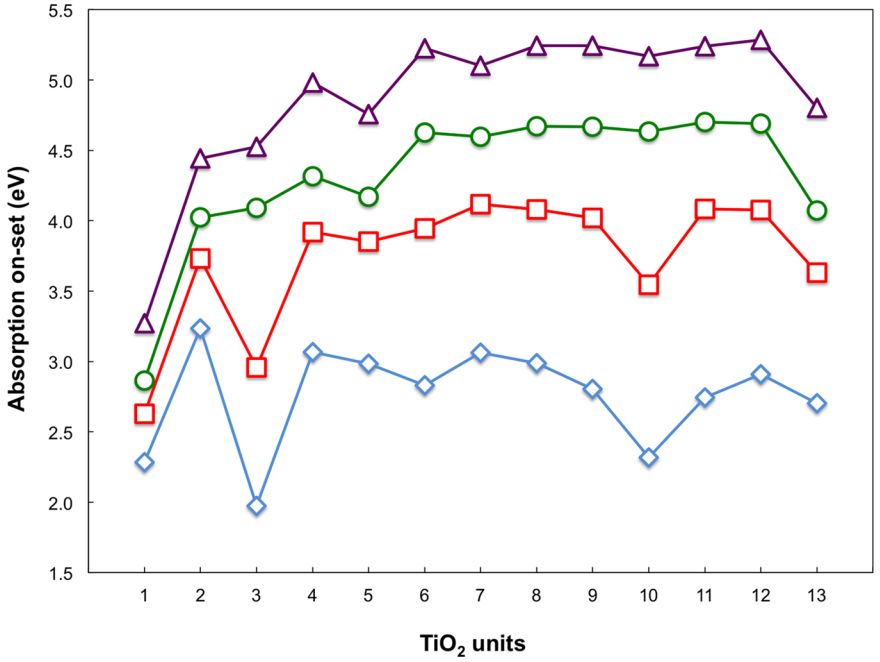

Figure 3. Lowest singlet excitation energies calculated with different TD-DFT XC potentials for the B3LYP/def2-TZVP optimized ground state $(TiO_2)_n$ GM structures. PBE values are represented by blue diamond markers, B3LYP red squares, CAMB3LYP green circles, and BHLYP excitations are displayed as purple triangles.

dx.doi.org/10.1021/ct4010273 | J. Chem. Theory Comput. 2014, 10, 1189−1199

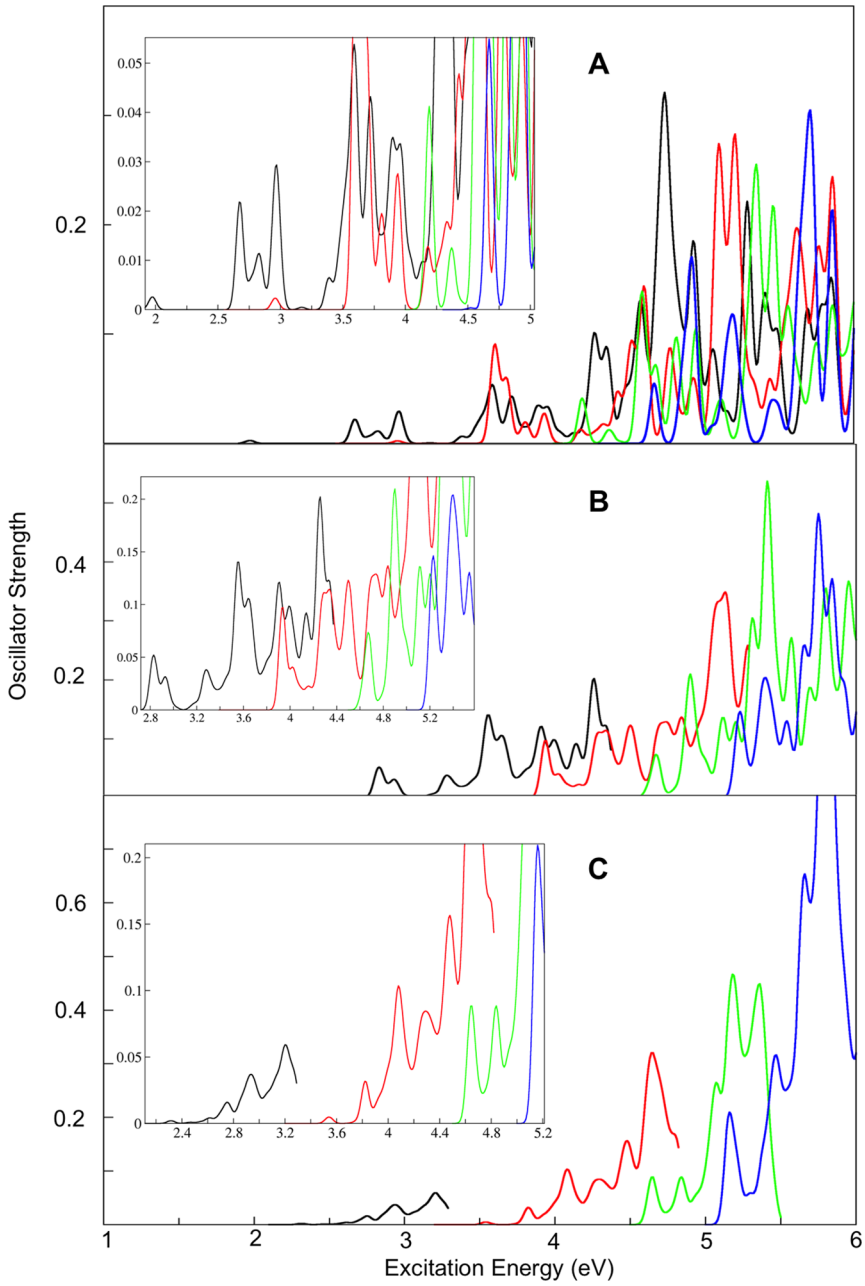

Figure 4. TD-DFT calculated optical spectra (100 lowest excitations, or 50 lowest in the case of TD-CAM-B3LYP for reasons of computational tractability) for (A) $(TiO_2)_3$ GM, (B) $(TiO_2)_6$ GM, and (C) $(TiO_2)_{10}$ GM optimized structures at the B3LYP/def2-TZVP level. In the top left of each spectrum, as insert is shown, with a zoom in of the low-energy part of the spectrum. The black line represents the TD-PBE results, the red one the TD-B3LYP, and the green one TD-CAM-B3LYP, while the blue one corresponds to the TD-BHLYP spectra. All excitations plotted are represented as Gaussians with a standard deviation of 0.03 eV.

3. RESULTS

In this section, we will first compare the lowest excitation energies of the $(TiO_2)_n$ GM clusters obtained with the four different TD-DFT XC potentials (PBE, B3LYP, BHLYP, and CAM-B3LYP). We will then investigate how the choice of the XC potential affects the shape of the TD-DFT optical spectrum, and in particular we compare the spectra of the $(TiO_2)_n$ clusters that show different trends in their excitations. Next, to further understand what is the origin of the differences between excitation energies calculated with various XC potentials, we investigate the excitation energies of a selection of small clusters (n = 1−5) with relevant defects using EOM-CC and compare the TD-DFT results (TD-B3LYP and TD-CAMB3LYP) with the EOM-CC benchmark values. Moreover, through the calculation of the Λ value we try to investigate the origin of the trends shown by the different XC potentials, further confirming the usefulness of this diagnostic test for the detection of possible charge transfer (CT) problems in TD-DFT. Finally, we define some EOM-CC benchmarks for hydrated structures and try to understand if after hydration the differences between the values predicted with the various XC potentials still persist.

3.1. TD-DFT Vertical Excitations for $(TiO_2)_n$. As shown in Figure 3, the four different XC potentials exhibit a similar trend in the description of the lowest excitation energy (S1, the absorption on-set) for the $(TiO_2)_n$ GM clusters. There appears

dx.doi.org/10.1021/ct4010273 | J. Chem. Theory Comput. 2014, 10, 1189−1199

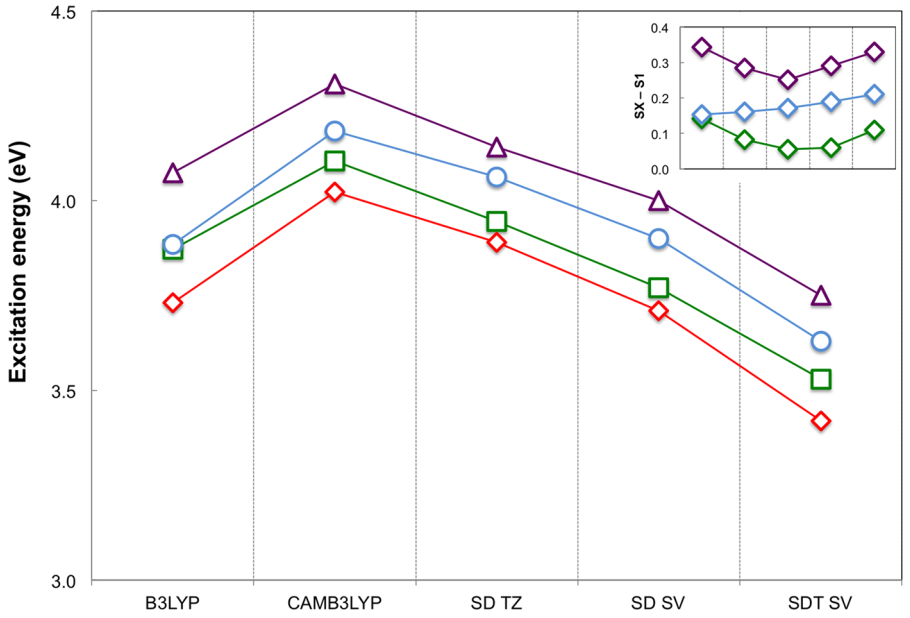

Figure 5. Trend in the four lowest excitation energies of the $(TiO_2)_2$ GM dimer cluster as calculated with different method combinations (1^1B_g red diamonds, 1^1A_u green squares, 1^1B_u blue circles, and 2^1A_g purple triangles). SD and SDT stand for EOM-CCSD/T, while SV and TZ correspond to the def2-SVP and def2-TZVPP basis sets. All of the TD-DFT calculations (B3LYP and CAM-B3LYP) employed the def2-TZVP basis set. All of the EOM-CC data shown were taken from our previous work.[32] The inset shows, for all the methods employed, the difference between the higher excited states (e.g., S4, S3, and S2) compared to the lowest excited energy S1.

to be a constant energy shift that is dependent upon the amount of exact HF-like exchange (HFLE) included in each of the XC potentials employed. For example, PBE with 0% HFLE gives the lowest excitation energies, while BHLYP with 50% of HFLE yields the highest values. Excitation energies obtained using B3LYP that has 20% HFLE, and, CAM-B3LYP, with 19% at short-range and 65% at long-range, lie in between the PBE and BHLYP values. However, aside from the similarities observed among the four data series, it is easy to see that the trend for TD-PBE and TD-B3LYP has two clear dips of ca. 0.5 eV, at $(TiO_2)_3$ and $(TiO_2)_{10}$, which are absent in the CAM-B3LYP and BHLYP results. In addition, the PBE XC potential results show a similar but smaller dip for the $(TiO_2)_6$ structure, while TD-B3LYP places this excitation in between the energies obtained for $(TiO_2)_5$ and $(TiO_2)_7$, and TD-CAM-B3LYP and TD-BHLYP predict a local maximum in the trend for this geometry. Both of the lowest excitations for the $(TiO_2)_3$ and $(TiO_2)_{10}$ clusters correspond to states with weak absorption intensity (i.e., low oscillator strength). However, it is important to stress that they are not dark states (excitations with zero absorption intensity); with TD-B3LYP the oscillator strengths are 9×10^{-5} (although 2 orders of magnitude weaker than the most intense excitation among the hundred lowest excitations) and 3.6×10^{-4} (1 order of magnitude weaker), respectively.

In agreement with the observations above, Figure S2.4 in section ESI-2 of the Supporting Information shows that there is a good linear fit between the TD-CAM-B3LYP and TD-BHLYP predicted absorption on-set values of the GM clusters (r^2 of 0.99, with r^2 being the coefficient of determination of the fit, which ranges between 0 and 1; as r^2 approaches 1, the quality of the fit improves), while the correlation between TD-CAM-B3LYP and TD-B3LYP absorption on-sets is much weaker (r^2 of 0.80). Not surprisingly, the clearest outliers in the latter case are the absorption on-set values for $(TiO_2)_3$ and $(TiO_2)_{10}$ GM clusters.

We also investigated the trends for the next two excited states (the second and third lowest singlet excitations, S2 and S3) for the same set of clusters (see values and graph in ESI-2). The trends found for these higher excited states are very similar to the ones observed for the lowest excited state shown in Figure 3. The two dips for the $(TiO_2)_3$ and $(TiO_2)_{10}$ structures are still there for the S2 and S3 states calculated with TD-PBE and TD-B3LYP. The S2 and S3 states for $(TiO_2)_3$ exhibit absorption intensities (as calculated with TD-B3LYP) 1 order of magnitude more intense than the lowest excitation, while for $(TiO_2)_{10}$ the S2 and S3 states have a weaker intensity compared to the S1 state. The underestimation of the excitation energies observed when using pure GGA XC potentials or hybrid XC potentials with a small HFLE contribution (e.g., B3LYP) is thus not limited to the lowest excited state, but it has an influence on higher energy states as well and therefore on the overall shape of the optical spectrum. In order to understand the size of this underestimation on the whole spectrum, we compared the shape of the optical spectra calculated with different XC potentials for the anomalous $(TiO_2)_3$ and $(TiO_2)_{10}$ clusters and the $(TiO_2)_6$ cluster as shown in Figure 4A–C (for all of the XC potentials employed, only the 2–6 eV excitation range is shown).

The different shapes of the spectra for $(TiO_2)_3$ emphasize the influence of the chosen XC potential. TD-PBE and TD-B3LYP XC potentials predict a weak shoulder at low energies (1.97 and 2.96 eV, respectively), followed by an approximate 0.7 eV gap to the next peak. In the case of TD-CAM-B3LYP and TD-BHLYP, no such large gap is observed, and the most intense peaks, for both of these XC potentials, seem to roughly agree after being rigidly shifted by ca. 0.5 eV. When the TD-B3LYP spectrum is shifted upward by ca. 1 eV and compared to the TD-CAM-B3LYP spectrum, we can clearly see that the two XC potentials show a poor agreement in the lower energy range of the spectrum, with B3LYP underestimating the first excitation energy and completely missing the lower energy

dx.doi.org/10.1021/ct4010273 | J. Chem. Theory Comput. 2014, 10, 1189–1199

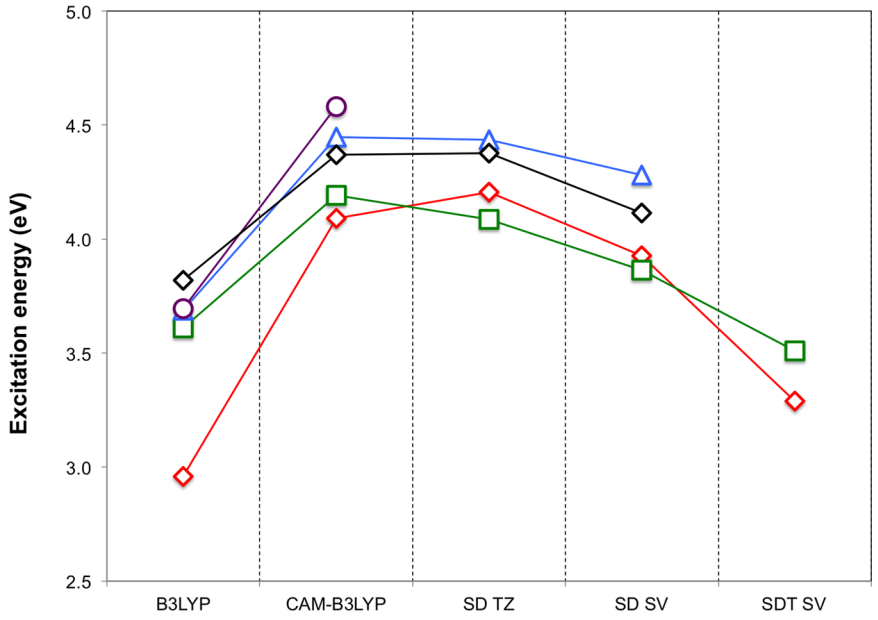

Figure 6. Trend in the five lowest excitation energies of the $(TiO_2)_3$ GM trimer as calculated with different method combinations ($2^1A'$ red diamond, $1^1A''$ green square, $3^1A'$ blue triangle, $4^1A'$ purple circle, and $2^1A''$ black diamond). SD and SDT stand for EOM-CCSD/T, while SV and TZ correspond to the def2-SVP and def2-TZVPP basis sets. All of the TD-DFT calculations (B3LYP and CAM-B3LYP) employed the def2-TZVP basis set. All of the EOM-CC data bar the EOM-CCSD TZ (SD TZ) excitation energies where taken from our previous work.[32]

features predicted by TD-CAM-B3LYP. The two XC potentials show a much better agreement at higher energies, and although the intensities do not match perfectly, all the peaks fall within the same range of energies. The TD-B3LYP, TD-CAM-B3LYP, and TD-BHLYP calculated spectra for the $n = 6$ GM cluster, after a rigid shift is applied, show a very good agreement on the position of the excitation peaks. A suitable shift could not be found in order to match the spectrum generated using the PBE XC potential. Finally, for the spectrum of the $(TiO_2)_{10}$ structure shown in Figure 4C, as expected, a similar behavior to the $(TiO_2)_3$ structure is observed. For example, the TD-PBE and TD-B3LYP calculated spectra show a very weak shoulder at lower energies, which, even after a rigid shift in energy, cannot be made to coincide with any of the peaks predicted by TD-CAM-B3LYP or TD-BHLYP.

3.2. TD-DFT vs EOM-CC for Naked Clusters. As observed in the previous section, the lowest energy excitation for the two $(TiO_2)_3$ and $(TiO_2)_{10}$ structures is described differently depending on the XC potential employed in the TD-DFT calculation. To benchmark the TD-DFT results, we now perform quantum chemical calculations. For reasons of computational tractability, we confine our investigation to clusters of a similar size to the $(TiO_2)_3$ cluster. Because the GM $(TiO_2)_3$ cluster exhibits a three-coordinated titanium atom and a three-coordinated oxygen atom, structural elements not present in the other GM for $n = 1-5$, we also consider metastable clusters of two and three TiO_2 units reported in the literature, which have similar coordination environments for titanium and/or oxygen atoms. This led us to include the so-called *club* structure, a $(TiO_2)_2$ isomer that is 0.73 eV (B3LYP/def2-TZVP) higher in energy than the $n = 2$ GM and a trimer isomer that lies 0.32 eV higher than the $n = 3$ GM. The latter has a three-coordinated titanium atom, and in contrast with the trimer GM, no three-coordinated oxygen atoms. For completeness, we also compared TD-DFT and EOM-CC excitations for another $(TiO_2)_2$ isomer, which is the *cis* version of the *trans* GM and lies 0.25 eV (B3LYP/def2-TZVP) in energy above it. All of these structures are shown in Figure 1.

In Figures 5 and 6, the four lowest excitation energies of the $(TiO_2)_2$ and $(TiO_2)_3$ global minima, respectively, are plotted as a function of the chosen energy definition, TD-DFT (B3LYP and CAM-B3LYP) and different flavors of EOM-CC: EOM-CCSD/TZ, EOM-CCSD/SV, and EOM-CCSDT/SV (with the exception of EOM-CCSD/TZ excitation energies for the $(TiO_2)_3$ GM cluster, EOM-CC data were taken from our previous work[32]). Care should be taken, when comparing absolute excitation energies, as the convergence with respect to basis sets (TZ or better) and CC excitation level (EOM-CCSDT or better) are currently only numerically feasible for the TiO_2 monomer, and even then supercomputing facilities are required (400−2000 cores per run with each core having at least on the order of 2 GB of memory). We thus focus instead primarily on the relative ordering of the different excitations, exploiting the fact that the clusters are highly symmetric and the excited states thus span a number of different irreducible representations.

The $(TiO_2)_2$ GM case in Figure 5 is representative for most small clusters. The same energetic ordering of the lowest excited states is observed for TD-DFT and the different EOM-CC flavors, with roughly similar energy differences between the different excited states (except that the gap between the S2 and S3 excited state for TD-B3LYP is much reduced; this is clearly shown in the inset of Figure 5, where for each method we plotted the energy of the SX state against the energy of the lowest excited state S1). The $(TiO_2)_3$ data in Figure 6 paint, however, a different picture, as there are a number of crossovers between the lowest excited states. We first compare the TD-B3LYP and TD-CAM-B3LYP results, which are, in line with the discussion above, very different. Not only is the energy difference between the S1 and S2 states reduced from 0.6 eV for TD-B3LYP to only 0.1 eV for TD-CAM-B3LYP, but the next couple of excited states lies much closer in energy for TD-B3LYP than for TD-CAM-B3LYP. Some of the higher lying

dx.doi.org/10.1021/ct4010273 | J. Chem. Theory Comput. 2014, 10, 1189−1199

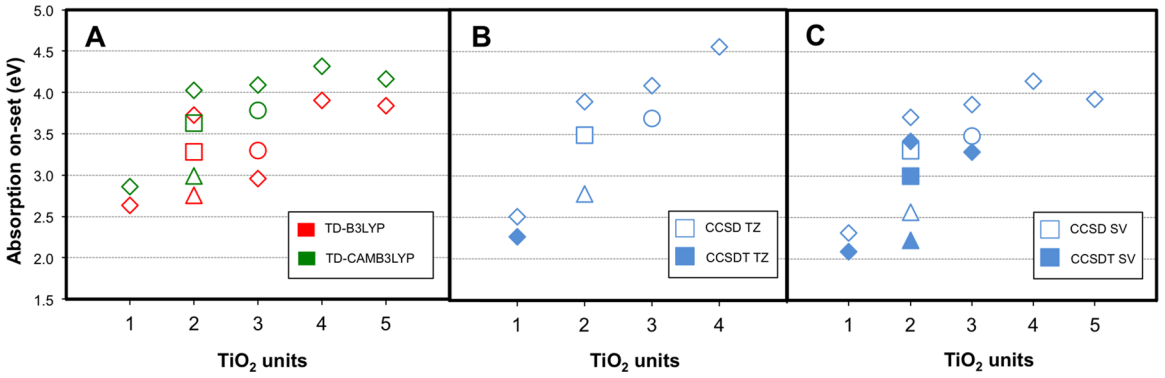

Figure 7. Comparison of TD-DFT excitation energies with EOM-CC results for a series of selected $(TiO_2)_n$ clusters, with n = 1−5. The global minima (GM) are represented by diamond markers, the metastable *cis* and *club* dimers by squares and triangles, respectively, and the metastable trimer (*alt*) by circles. (A) Comparison of TD-CAMB3LYP (green markers) and TD-B3LYP (red) excitations. (B) Comparison between EOM-CCSD and EOM-CCSDT results with the high quality TZ basis set. (C) Comparison between EOM-CCSD and EOM-CCSDT results with the small SV basis set.

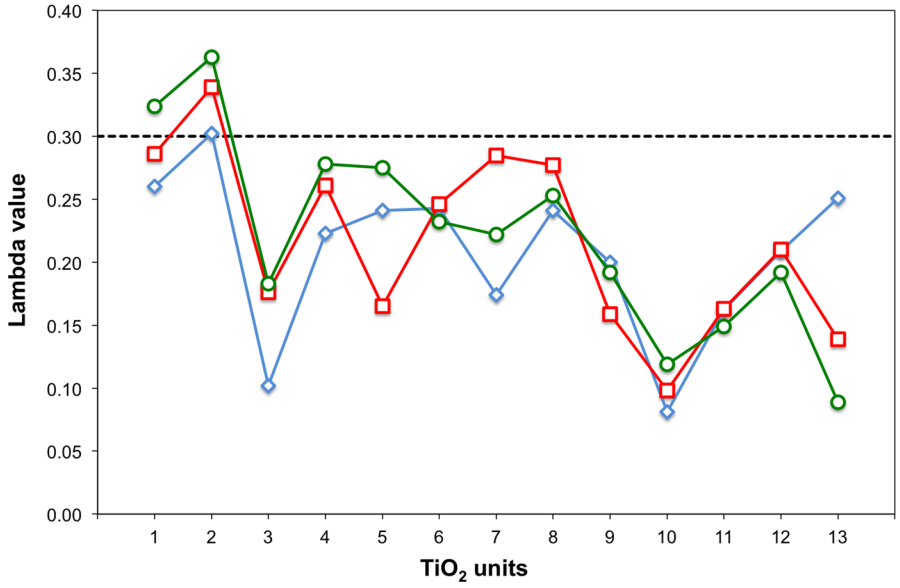

Figure 8. Λ values for the three lowest excited states (lowest state shown by blue diamonds, second lowest state by red squares, and third lowest state by green circles) of $(TiO_2)_n$ clusters, with n = 1−13, calculated with B3LYP XC potential. The dashed black line shows the Λ threshold defined by Peach et al. for organic systems.[66]

excited states effectively become degenerate in the case of TD-B3LYP and show a different ordering than found with TD-CAM-B3LYP. The TD-CAM-B3LYP and all EOM-CC results, in contrast, are very similar (with the exception of an interchange between the close-lying S1/S2 states for both sets of EOM-CCSD results).

Having compared the energies of different excited states of individual clusters, we now compare the excitation energies between the ground and lowest excited states for sets of clusters. Again, we perform calculations both with TD-DFT (TD-B3LYP and TD-CAM-B3LYP) and EOM-CC methods (EOM-CCSDT/SV up to $(TiO_2)_3$, EOM-CCSD/TZ up to $(TiO_2)_4$, and EOM-CCSD/SV up to $(TiO_2)_5$). Figure 7A contains the TD-DFT results and Figure 7B and C the EOM-CCSD/T TZ and EOM-CCSD/T SV data, respectively. Overall, TD-DFT and EOM-CC predict similar magnitudes of excitation energies as well as a similar ordering of the lowest excited states of the different clusters. For example, all methods employed here predict the same ordering of the lowest energy excitations of the dimer and monomer (*trans* > *cis* > *club* > monomer). TD-DFT and EOM-CCSD/SV also agree on where the lowest excitation energies of $(TiO_2)_4$ and $(TiO_2)_5$ global minima lie relative to that of the dimer. However, for the $(TiO_2)_3$ GM cluster, the different methods give widely different results. In agreement with EOM-CCSD, TD-CAM-B3LYP predicts that the lowest excitation energy of the $(TiO_2)_3$ GM to be slightly higher than that for the $(TiO_2)_2$ GM. In contrast, TD-B3LYP places the $(TiO_2)_3$ GM lowest excitation in a similar energy range as the lowest excitation of the $(TiO_2)_2$ *club* isomer and below the *alt* trimer. EOM-CCSD/TZ and EOM-CCSD/SV predict that the lowest excitation energy of the $(TiO_2)_3$ GM lies slightly higher than that of the $(TiO_2)_2$ GM, while EOM-CCSDT/SV puts the lowest excitation energy of the $(TiO_2)_3$ GM slightly below that of the $(TiO_2)_2$ GM.

Overall, both in terms of the relative energies of different excitations of the clusters and between different clusters, EOM-CC calculations suggest that TD-DFT does a reasonable job in describing electronic excitations of TiO_2 clusters. However, XC potentials with no or low percentages of HFLE, such as PBE and B3LYP, struggle for specific structures. TD-CAM-B3LYP

dx.doi.org/10.1021/ct4010273 | J. Chem. Theory Comput. 2014, 10, 1189−1199

(and TD-BHLYP), in contrast, yields lowest excitation energies qualitatively consistent with EOM-CC for all structures studied. Finally, when considering absolute excitation energies, taking into account the caveats discussed above, those obtained with TD-CAM-B3LYP lie generally quantitatively closest to the EOM-CC data. We, therefore, would recommend using this XC potential, where possible, to model excited state processes in TiO_2 nanoparticles.

3.3. The Charge Transfer Character of the TD-DFT Excitations. It is well-known that the use of standard XC potentials with no HFLE (i.e., GGA) or a low percentage of HFLE (e.g., B3LYP) in TD-DFT can result in the underestimation of charge transfer (CT) excitations, where the origin and final destination of the excited electron are separated spatially. It is appealing to suppose that this erroneous energetic stabilization of CT states might be the origin of the discrepancy between TD-PBE and TD-B3LYP on one hand and TD-CAM-B3LYP, TD-BHLYP, and EOM-CC on the other hand. Hence, it is important to try to characterize the CT character of the excitations for the different nanoclusters, as calculated with TD-DFT. In this section, we thus employ the Λ diagnostic suggested by Peach et al.[66] This diagnostic quantifies the spatial overlap between the (unperturbed) occupied and virtual orbitals involved in the TD-DFT excitation and hence is an estimate of the CT character of a specific excitation. The Λ value corresponds to a dimensionless number, which varies from 0 (no overlap between the occupied and virtual orbitals responsible for a TD-DFT excitation) to 1 (complete overlap between the occupied and virtual orbitals).

In the original paper by Peach et al.,[66] it is suggested that a TD-DFT excitation with small Λ may be associated with large CT errors, while in contrast small CT errors are associated with large Λ. In this fashion, the authors imply that, for example, TD-PBE excitations with $\Lambda < 0.4$ or TD-B3LYP excitations with $\Lambda < 0.3$ are likely to contain a significant error, while for TD-CAM-B3LYP no correlation is observed between errors and spatial overlap, as measured by Λ.[66] These limits, however, have been obtained for a set of organic molecules, and to our knowledge no one has yet published similar thresholds for inorganic systems, e.g., metal oxides.

Figure 8 shows Λ values calculated with TD-B3LYP for the three lowest excitations obtained for the $n = 1-13$ GM $(TiO_2)_n$ clusters. We calculated the Λ values also for the PBE, CAM-B3LYP, and BHLYP XC potentials for all the GMs and the metastable isomers, see the Supporting Information ESI-2. For the lowest excited state (S1, blue diamonds in Figure 8), all of the TD-B3LYP values lie below the threshold (0.30) defined by Peach et al. for hybrid XC potentials. However, among the Λ values calculated for the S1 state using TD-B3LYP, perhaps not surprisingly, both the $(TiO_2)_3$ and $(TiO_2)_{10}$ GM clusters are clearly the lowest, with some other clusters, $(TiO_2)_7$, $(TiO_2)_{11}$, and $(TiO_2)_9$, showing moderately low values as well. For the non-GM structures, the *alt* trimer has the lowest Λ value. Λ values for the higher excited states (S2 and S3), as shown in Figure 8, can be, depending on the particular cluster, both larger and smaller than that of S1. Examples of clusters with Λ values for higher excited states that lie below their S1 counterparts include $(TiO_2)_5$ (S2), $(TiO_2)_9$ (S2), and $(TiO_2)_{13}$ (S3).

The Λ data for our titania clusters yield a number of interesting observations. First, all of the Λ values for the TiO_2 clusters are smaller than typical Λ values for organic systems, i.e. the TiO_2 clusters consistently have a smaller overlap of the orbitals involved in the excitation. We believe that this arises from the fact that excitations in inorganic systems, such as TiO_2, typically involve the displacement of an electron from one sublattice (using the term lattice loosely) to another sublattice, here from orbitals based on oxygen atoms to those based on titanium atoms. In such a scenario, even local excitations (i.e., excitations where both centers involved are spatially close) might have low Λ values, especially if the material is rather ionic and there is thus only limited overlap between orbitals on either sublattice. The good qualitative fit between the TD-DFT and EOM-CC results for excitations with Λ values between 0.15 and 0.3 strongly suggests that these are not excitations which are badly described by XC potentials due to CT related problems. A more interesting observation is that the excitations for which the description is problematic with TD-PBE and TD-B3LYP, both relative to that in TD-CAM-B3LYP and TD-BHLYP and to that by EOM-CC, are the same excitations that have very low Λ. This observation suggests that the reason why the description of these specific excitations is problematic within TD-PBE and TD-B3LYP is that they have an especially strong CT character, and hence the states involved are erroneously stabilized, i.e., lie lower in energy relative to the S0 ground state than they should.

This erroneous stabilization is not limited to the lowest excitation. For example, as outlined above, the second excitation (S2) of the $(TiO_2)_5$ structure has a rather low Λ value, substantially lower than that of S1 and S3, and it is interesting to compare in this context the predictions of TD-B3LYP with those obtained with other methods. The S2 excited state in TD-B3LYP belongs to the A″ irreducible representation (just as S0 and S1, and hence it can be labeled as the $3^1A''$ state), while in EOM-CC (and in TD-CAM-B3LYP and TD-BHLYP) S2 belongs to the A′ irreducible representation (the $1^1A'$ state) and S3 in contrast is the $3^1A''$ state. This swap in the energetic ordering of the lowest two states is probably a direct result of the erroneous CT related stabilization of the $3^1A''$ state in TD-B3LYP, which shifts it below the $1^1A'$ state.

3.4. The Microscopic Picture. A close inspection of the atomic structures of the clusters studied, the orbitals involved in the excitations and the ground state−excited state density differences, suggests that the problematic CT excitations typically involve one or more singly coordinated oxygen atoms as the origin of the excited electron and hence the location of the formed hole. The structural fragment on which the excited electron localizes varies and can be, for instance, a titanium atom with nominally only three oxygen atoms in its first coordination sphere (as found for the $(TiO_2)_3$ GM and $(TiO_2)_2$ *club* structures, see Figure 9) or a fragment constituted of three four-coordinated titanium atoms surrounding a common three-coordinated oxygen atom (as found for the $(TiO_2)_{10}$ GM structure, see Figure 10). The latter combination of atoms is superficially similar to that of one-half of the Valence Alternation Pair (VAP) defect-pair in silica nanostructures.[69] The presence of these structural fragments, however, is no guarantee that the lowest excitations will have CT character. This is illustrated, for example, by the case of the $(TiO_2)_2$ *club* isomer (see Figure 9). This structure has both a singly coordinated oxygen atom and a triply coordinated titanium atom, but its lowest three excitations all have reasonable TD-B3LYP Λ values (see ESI-2), and their TD-B3LYP excitation energies qualitatively agree with EOM-CC results.

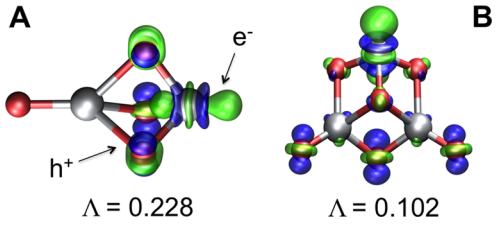

Figure 9. TD-B3LYP lowest singlet excited state density difference and Λ value obtained for (A) the *club* dimer and (B) the GM trimer. In both pictures, the green lobes represent regions of excess electron density (where the excited electron component of the excited state is located, $\mathbf{e}^-$), whereas the blue lobes represent regions deficient in electron density (where the hole component is found, $\mathbf{h}^+$).

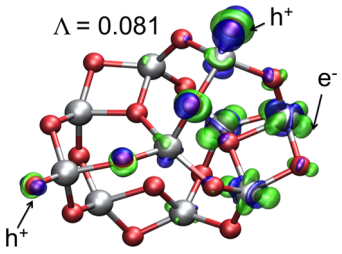

Figure 10. TD-B3LYP lowest singlet excited state density difference and Λ value obtained for the $(TiO_2)_{10}$ structure. The green lobes represent excess regions of electron density (where the excited electron component of the excited state is located, $\mathbf{e}^-$), whereas the blue lobes represent regions deficient in electron density (where the hole is found, $\mathbf{h}^+$).

When rationalizing the above observations, we have to make a choice between a semi-ionic or a semicovalent reference frame. In the latter reference, one can think of low-energy excitations as the transfer of an electron between two well-defined centers that deviate electronically and structurally from the bonding pattern in the remainder of the particle (e.g., the silanone,[44,70,71] Si^+-O^-, nonbridging oxygens,[72,73] Si−O*, and siloxy, $Si-O^-$ centers in silica). In contrast, in the semi-ionic reference, the "centres" involved in low-energy excitations are much less well-defined and importantly much less obvious upon inspection. The hole and electron component of an excitation could be smeared out over a number of ions, with the precise ions involved (i.e., localization sites) governed by a subtle interplay between the on-site electrostatic potential (the energetic cost of adding or removing an electron from a specific ion) and the electrostatic interaction between the excited electron and the remaining hole (i.e., the exciton binding energy). Intuitively, the latter picture seems closer to what we observe for $(TiO_2)_n$ nanoparticles. The wide range of first coordination Ti−O distances in the clusters, and the fact that the Ti−O distances for the singly coordinated oxygen atoms are always virtually the same (1.6 Å), independent of the coordination number of the nearest titanium atom, also suggests that the semi-ionic reference frame is the most apt description of TiO_2 nanoparticles. While in this picture, it is relatively difficult to link structure to excitations, there is one important thing we can note. While singly coordinated oxygen atoms have generally the lowest on-site electrostatic (or Madelung) potential and are the centers from which an electron gets removed if one does a single-point calculation for the cation, this does not mean, however, that it will be involved in the lowest energy excitation (or more generally in low energy excitations). For example, for $(TiO_2)_4$ the first two lowest excitations do not involve the singly coordinated oxygen atoms, while for $(TiO_2)_5$ only the second excitation (with TD-B3LYP, see discussion in section 3.3 and Figure S-2.3 of the ESI-2.5) involves the singly coordinated oxygen atom. The lowest excitation of the $(TiO_2)_2$ *club* dimer, also, does not involve the singly coordinated atom (see Figure 9). The hole and excited electron in this case are localized in close proximity, maximizing excited electron−hole overlap (Λ, see above) and minimizing the charge-transfer character of the excitation. Clearly, there is thus a subtle balance between the on-site electrostatic potential and the electrostatic interaction between electron and hole,

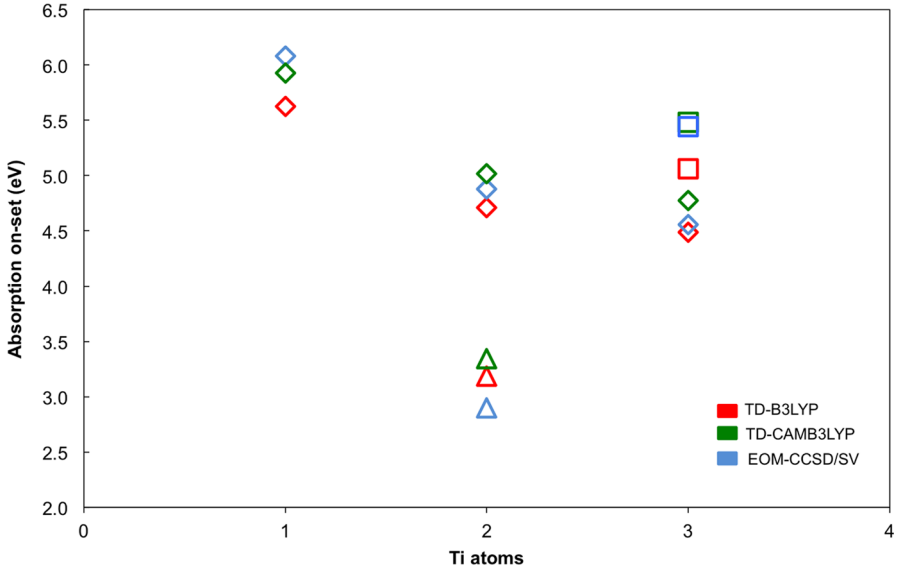

Figure 11. Comparison between TD-DFT (B3LYP, red markers and CAM-B3LYP, green markers) lowest singlet excitations and EOM-CCSD def2-SV(P) (blue markers) for hydrated $(TiO_2)_n(H_2O)_m$ systems, where n and m range between 1 and 3. The diamond markers represent the $Ti(OH)_4$, $(TiO_2)_2(H_2O)_2$, and $(TiO_2)_3(H_2O)_2$ structures, respectively; the triangle marker, the $(TiO_2)_2H_2O$ cluster; and the square, the $(TiO_2)_3(H_2O)_3$ cluster.

dx.doi.org/10.1021/ct4010273 | J. Chem. Theory Comput. 2014, 10, 1189−1199

where the latter in practice is sufficiently strong to change which parts of the cluster are involved in low energy excitations.

Taking into account the discussion above, it is likely that the location of the excited electron and hole will change during excited state processes that involve nuclear displacement (e.g., relaxation). As a result, the electronic character of an excitation, its Λ value, and the ability of TD-DFT to correctly describe the excitation might also change. In future work, we will, therefore, study this explicitly. Here, however, it is important to note that without a correct description of the (energetic ordering of the) lowest excited states at the ground state geometry, one has no hope of describing what happens upon moving away from this starting point on the excited-state energy landscape.

3.5. Hydrated Clusters: TD-DFT vs EOM-CC. Upon hydration, all the centers discussed above (i.e., singly coordinated oxygen atoms and under-coordinated titanium atoms) are saturated by the addition of hydroxyl groups ($-OH^-$) and protons (H^+). Hydration is strongly exothermic (e.g., −250 kJ/(mol H_2O) in the case of $(TiO_2)_2$, in line with previous estimates from the literature[74]). As structural and electronic features of the naked systems are modified, so are the orbitals involved in the optical excitation. In Figure 11, we present the comparison between the TD-B3LYP, TD-CAM-B3LYP, and EOM-CCSD SV absorption on-set for a series of hydrated $(TiO_2)_n(H_2O)_m$ systems, where n and m range from 1−3. The addition of water to the naked clusters results in a blue shift of their optical spectra. Figure 11 also shows, in line with that discussed above, how the CAM-B3LYP excitations always lie at higher energies than their B3LYP counterparts, with a mean difference of 0.29 eV. It is important to notice that, unlike what is observed for specific naked structures (e.g., $(TiO_2)_3$ and $(TiO_2)_{10}$), we found a generally good agreement between B3LYP and CAM-B3LYP excitations for all hydrated clusters. In this case, the Λ values computed for the B3LYP excitations for the hydrated clusters are generally higher than those calculated for the naked clusters (values listed in the ESI-4). Moreover, the TD-DFT results with both XC potentials show a generally good agreement with those obtained using EOM-CCSD/SV, with an average absolute difference of 0.27 eV for B3LYP and 0.20 eV for CAM-B3LYP. Thus, hydration seems to effectively remove the centers responsible for the problematic CT excitations and, more importantly, suggests that TD-B3LYP in general will give good results for hydrated systems.

5. CONCLUSIONS

In this paper, we have studied the suitability of TD-DFT to describe low-energy excitations in TiO_2 nanoparticles through a comparison with EOM-CC quantum chemistry calculations. We find that TD-DFT generally gives a good qualitative and also, in the case of TD-B3LYP and TD-CAM-B3LYP, a quantitative fit to excitation energies predicted by the more accurate, but computationally much more expensive, EOM-CC method. However, for selected particles, e.g., the $(TiO_2)_3$ GM cluster, we observe large deviations from EOM-CC results when using the TD-PBE and TD-B3LYP XC potentials. Calculation of Λ, which provides a measure of the orbital overlap between the orbitals involved in the excitation, and visual inspection of the excited-state density differences in these cases suggests that problems arise for these systems when computing charge-transfer excitations, the energy of which relative to local excitations is underestimated by TD-PBE and TD-B3LYP. Such problems are completely absent for TD-CAM-B3LYP and TD-BHLYP. On the basis of this and the overall good quantitative fit of TD-CAM-B3LYP and EOM-CC results, we recommend using this XC potential, where possible, when studying excitations in TiO_2 nanoparticles. Finally, hydration of these particles removes the structural centers responsible for the problematic charge-transfer excitations, and all XC potentials studied here yield a good qualitative fit to EOM-CC results for hydrated particles.

■ ASSOCIATED CONTENT

Ⓢ Supporting Information

Geometries of all the $(TiO_2)_n$ naked and hydrated clusters optimized at the B3LYP/def2-TZVP level; TD-DFT and EOM-CC lowest excitation energies for all the naked and hydrated $(TiO_2)_n$ clusters studied in this work; leading orbital contributions to the two lowest energy excitations for the $(TiO_2)_3$ GM cluster calculated with various XC potentials in TD-DFT; TD-B3LYP excited state density difference for the lowest states of the $(TiO_2)_4$ and $(TiO_2)_5$ GM naked clusters and of all the hydrated structures; comparison of the TD-B3LYP and TD-BHLYP excitation energies plotted against the TD-CAM-B3LYP values for all of the naked clusters. This material is available free of charge via the Internet at http://pubs.acs.org/.

■ AUTHOR INFORMATION

Corresponding Author

*E-mail: m.zwijnenburg@ucl.ac.uk.

Notes

The authors declare no competing financial interest.

■ ACKNOWLEDGMENTS

We kindly acknowledge Prof. S. T. Bromley, Dr. M. Calatayud, Dr. A. Kerridge, Prof. A. Shluger, Dr. A. A. Sokol, and Dr. C. Sousa for stimulating discussions. M.A.Z. acknowledges the UK Engineering and Physical Sciences Research Council (EPSRC) for a Career Acceleration Fellowship (Grant EP/I004424/1). This study has further been supported by a UCL Impact studentship award to E.B. Computational time on the computers of the Unity High Performance Computing Facility at University College London, the IRIDIS regional high-performance computing service provided by the e-Infrastructure South Centre for Innovation (EPSRC Grants EP/K000144/1 and EP/K000136/1) and on HECToR, the U.K.'s national high-performance computing service (via our membership in the UK's HPC Materials Chemistry Consortium, which is funded by EPSRC grants EP/F067496/1 and EP/L000202/1), is gratefully acknowledged. A significant portion of the research was also performed using PNNL Institutional Computing at Pacific Northwest National Laboratory and EMSL, a national scientific user facility sponsored by the Department of Energy's Office of Biological and Environmental Research and located at Pacific Northwest National Laboratory. The Pacific Northwest National Laboratory is operated for the U.S. Department of Energy by the Battelle Memorial Institute under Contract DEAC06.76RLO-1830.

■ REFERENCES

(1) Fujishima, A.; Honda, K. *Nature* **1972**, *238*, 37.
(2) Satoh, N.; Nakashima, T.; Kamikura, K.; Yamamoto, K. *Nat. Nanotechnol.* **2008**, *3*, 106.
(3) Monticone, S.; Tufeu, R.; Kanaev, A. V.; Scolan, E.; Sanchez, C. *Appl. Surf. Sci.* **2000**, *162*−*163*, 565.

(4) Anpo, M.; Shima, T.; Kodama, S.; Kubokawa, Y. *J. Phys. Chem.* **1987**, *91*, 4305.
(5) Tachikawa, T.; Fujitsuka, M.; Majima, T. *J. Phys. Chem. C* **2007**, *111*, 5259.
(6) Gratzel, M. *Nature* **2001**, *414*, 338.
(7) Ni, M.; Leung, M. K. H.; Leung, D. Y. C.; Sumathy, K. *Renew. Sust. Energy Rev.* **2007**, *11*, 401.
(8) Jagadale, T. C.; Takale, S. P.; Sonawane, R. S.; Joshi, H. M.; Patil, S. I.; Kale, B. B.; Ogale, S. B. *J. Phys. Chem. C* **2008**, *112*, 14595.
(9) Schrauzer, G. N.; Guth, T. D. *J. Am. Chem. Soc.* **1977**, *99*, 7189.
(10) Biswas, A.; Corani, A.; Kathiravan, A.; Infahsaeng, Y.; Yartsev, A.; Sundstrom, V.; De, S. *Nanotechnology* **2013**, *24*, 195601.
(11) Cernuto, G.; Masciocchi, N.; Cervellino, A.; Colonna, G. M.; Guagliardi, A. *J. Am. Chem. Soc.* **2011**, *133*, 3114.
(12) Murakami, N.; Kurihara, Y.; Tsubota, T.; Ohno, T. *J. Phys. Chem. C* **2009**, *113*, 3062.
(13) Amano, F.; Prieto-Mahaney, O.-O.; Terada, Y.; Yasumoto, T.; Shibayama, T.; Ohtani, B. *Chem. Mater.* **2009**, *21*, 2601.
(14) Cho, C. H.; Han, M. H.; Kim, D. H.; Kim, D. K. *Mater. Chem. Phys.* **2005**, *92*, 104.
(15) Li, Y.-F.; Liu, Z.-P. *J. Am. Ceram. Soc.* **2011**, *133*, 15743.
(16) Persson, P.; Bergstrom, R.; Lunell, S. *J. Phys. Chem. B* **2000**, *104*, 10348.
(17) Di Valentin, C.; Pacchioni, G.; Selloni, A. *Phys. Rev. B* **2004**, *70*, 85116.
(18) Li, S.; Dixon, D. A. *J. Phys. Chem. A* **2008**, *112*, 6646.
(19) De Angelis, F.; Fantacci, S.; Selloni, A. *Nanotechnology* **2008**, *19*, 424002.
(20) Rocca, D.; Gebauer, R.; De Angelis, F.; Nazeeruddin, M. K.; Baroni, S. *Chem. Phys. Lett.* **2009**, *475*, 49.
(21) Blagojevic, V.; Chen, Y. R.; Steigerwald, M.; Brus, L.; Friesner, R. A. *J. Phys. Chem. C* **2009**, *113*, 19806.
(22) Shevlin, S. A.; Woodley, S. M. *J. Phys. Chem. C* **2010**, *114*, 17333.
(23) Chiodo, L.; Maria Garcia-Lastra, J.; Iacomino, A.; Ossicini, S.; Zhao, J.; Petek, H.; Rubio, A. *Phys. Rev. B* **2010**, *82*, 45207.
(24) Wang, T. H.; Fang, Z.; Gist, N. W.; Li, S.; Dixon, D. A.; Gole, J. L. *J. Phys. Chem. C* **2011**, *115*, 9344.
(25) Auvinen, S.; Alatalo, M.; Haario, H.; Jalava, J. P.; Lamminmäki, R. J. *J. Phys. Chem. C* **2011**, *115*, 8484.
(26) Marom, N.; Moussa, J. E.; Ren, X.; Tkatchenko, A.; Chelikowsky, J. R. *Phys. Rev. B* **2011**, *84*, 245115.
(27) Zhang, J.; Hughes, T. F.; Steigerwald, M.; Brus, L.; Friesner, R. A. *J. Am. Chem. Soc.* **2012**, *134*, 12028.
(28) Li, J.; Wang, H.; Persson, P.; Thoss, M. *J. Chem. Phys.* **2012**, *137*, 22A529.
(29) Nunzi, F.; Mosconi, E.; Storchi, L.; Ronca, E.; Selloni, A.; Grätzel, M.; De Angelis, F. *Energy Environ. Sci.* **2013**, *6*, 1221.
(30) Scanlon, D. O.; Dunnill, C. W.; Buckeridge, J.; Shevlin, S. A.; Logsdail, A. J.; Woodley, S. M.; Catlow, C. R. A.; Powell, M. J.; Palgrave, R. G.; Parkin, I. P.; Watson, G. W.; Keal, T. W.; Sherwood, P.; Walsh, A.; Sokol, A. A. *Nat. Mater.* **2013**, *12*, 798.
(31) Galynska, M.; Persson, P. *Int. J. Quantum Chem.* **2013**, *113*, 2611.
(32) Berardo, E.; Hu, H. S.; Kowalski, K.; Zwijnenburg, M. A. *J. Chem. Phys.* **2013**, *139*, 64313.
(33) Taylor, D. J.; Paterson, M. J. *J. Chem. Phys.* **2010**, *133*, 204302.
(34) Lin, C.-K.; Li, J.; Tu, Z.; Li, X.; Hayashi, M.; Lin, S. H. *R. Soc. Chem. Adv.* **2011**, *1*, 1228.
(35) Taylor, D. J.; Paterson, M. J. *Chem. Phys.* **2012**, *408*, 1.
(36) Chiodo, L.; Salazar, M.; Romero, A. H.; Laricchia, S.; Della Sala, F.; Rubio, A. *J. Phys. Chem.* **2011**, *135*, 244704.
(37) Marom, N.; Kim, M.; Chelikowsky, J. R. *Phys. Rev. Lett.* **2012**, *108*, 106801.
(38) Kasha, M. *Faraday Discuss.* **1950**, *9*, 14.
(39) Zwijnenburg, M. A. *Nanoscale* **2011**, *3*, 3780.
(40) Zwijnenburg, M. A.; Illas, F.; Bromley, S. T. *Phys. Chem. Chem. Phys.* **2011**, *13*, 9311.
(41) Zwijnenburg, M. A.; Sousa, C.; Illas, F.; Bromley, S. T. *J. Chem. Phys.* **2011**, *134*, 64511.
(42) Zwijnenburg, M. A. *Nanoscale* **2012**, *4*, 3711.
(43) Zwijnenburg, M. A. *Phys. Chem. Chem. Phys.* **2013**, *15*, 11119.
(44) Zwijnenburg, M. A.; Sokol, A. A.; Sousa, C.; Bromley, S. T. *J. Chem. Phys.* **2009**, *131*, 34705.
(45) Zhang, R.-Q.; De Sarkar, A.; Niehaus, T. A.; Frauenheim, T. *Phys. Status Solidi B* **2012**, *249*, 401.
(46) Wang, Y.; Zhang, R.; Frauenheim, T.; Niehaus, T. A. *J. Phys. Chem. C* **2009**, *113*, 12935.
(47) Wang, X.; Zhang, R. Q.; Lee, S. T.; Frauenheim, T.; Niehaus, T. A. *Appl. Phys. Lett.* **2008**, *93*, 243120.
(48) Sundholm, D. *Phys. Chem. Chem. Phys.* **2004**, *6*, 2044.
(49) Becke, A. D. *J. Chem. Phys.* **1993**, *98*, 5648.
(50) Weigend, F.; Ahlrichs, R. *Phys. Chem. Chem. Phys.* **2005**, *7*, 3297.
(51) Wu, H. B.; Wang, L. S. *J. Chem. Phys.* **1997**, *107*, 8221.
(52) Hamad, S.; Catlow, C. R. A.; Woodley, S. M.; Lago, S.; Mejias, J. A. *J. Phys. Chem. B* **2005**, *109*, 15741.
(53) Qu, Z. W.; Kroes, G. J. *J. Phys. Chem. B* **2006**, *110*, 8998.
(54) Calatayud, M.; Maldonado, L.; Minot, C. *J. Phys. Chem. C* **2008**, *112*, 16087.
(55) Syzgantseva, O. A.; Gonzalez-Navarrete, P.; Calatayud, M.; Bromley, S.; Minot, C. *J. Phys. Chem. C* **2011**, *115*, 15890.
(56) Chen, M.; Dixon, D. A. *J. Chem. Theory Comput.* **2013**, *9*, 3189.
(57) Perdew, J. P.; Burke, K.; Ernzerhof, M. *Phys. Rev. Lett.* **1996**, *77*, 3865.
(58) Yanai, T.; Tew, D. P.; Handy, N. C. *Chem. Phys. Lett.* **2004**, *393*, 51.
(59) Comeau, D. C.; Bartlett, R. J. *Chem. Phys. Lett.* **1993**, *207*, 414.
(60) Watts, J. D.; Bartlett, R. J. *J. Chem. Phys.* **1994**, *101*, 3073.
(61) Schafer, A.; Horn, H.; Ahlrichs, R. *J. Chem. Phys.* **1992**, *97*, 2571.
(62) Ahlrichs, R.; Bar, M.; Haser, M.; Horn, H.; Kolmel, C. *Chem. Phys. Lett.* **1989**, *162*, 165.
(63) Schmidt, M. W.; Baldridge, K. K.; Boatz, J. A.; Elbert, S. T.; Gordon, M. S.; Jensen, J. H.; Koseki, S.; Matsunaga, N.; Nguyen, K. A.; Su, S. J.; Windus, T. L.; Dupuis, M.; Montgomery, J. A. *J. Comput. Chem.* **1993**, *14*, 1347.
(64) Lai, P.-W.; Zhang, H.; Rajbhandari, S.; Valeev, E.; Kowalski, K.; Sadayappan, P. In *Proceedings of the International Conference on Computational Science, ICCS 2012*; Ali, H., Shi, Y., Khazanchi, D., Lees, M., VanAlbada, G. D., Dongarra, J., Sloot, P. M. A., Eds.; Springer: New York, 2012; Vol. *9*, p 412.
(65) Valiev, M.; Bylaska, E. J.; Govind, N.; Kowalski, K.; Straatsma, T. P.; Van Dam, H. J. J.; Wang, D.; Nieplocha, J.; Apra, E.; Windus, T. L.; de Jong, W. A. *Comput. Phys. Commun.* **2010**, *181*, 1477.
(66) Peach, M. J. G.; Benfield, P.; Helgaker, T.; Tozer, D. J. *J. Chem. Phys.* **2008**, *128*, 44118.
(67) *The Pymol Molecular Graphics System*, version 1.4.1; Schrödinger, LLC: Portland, OR, 2010.
(68) Humphrey, W.; Dalke, A.; Schulten, K. *J. Mol. Graphics Modell.* **1996**, *14*, 33.
(69) Zwijnenburg, M. A.; Illas, F.; Bromley, S. T. *J. Chem. Phys.* **2012**, *137*, No. 154313.
(70) Avakyan, V. G.; Sidorkin, V. F.; Belogolova, E. F.; Guselnikov, S. L.; Gusel'nikov, L. E. *Organometallics* **2006**, *25*, 6007.
(71) Radzig, V. A. *Colloids Surf., A* **1993**, *74*, 91.
(72) Giordano, L.; Sushko, P. V.; Pacchioni, G.; Shluger, A. L. *Phys. Rev. Lett.* **2007**, *99*, 136801.
(73) Suzuki, T.; Skuja, L.; Kajihara, K.; Hirano, M.; Kamiya, T.; Hosono, H. *Phys. Rev. Lett.* **2003**, *90*, 186404.
(74) Pandey, L. B.; Aikens, C. M. *J. Phys. Chem. A* **2012**, *116*, 526.